

# Sol-gel Preparation of Photocatalytic $\text{Sm}_2\text{Ti}_2\text{O}_7/\text{HZSM-5}$ Composite on Degradation of Reactive Brilliant Red X-3B

Wenjie ZHANG\*, Yuxuan LIU, Ling DU

School of Environmental and Chemical Engineering, Shenyang Ligong University, Shenyang 110159, China

**crossref** <http://dx.doi.org/10.5755/j01.ms.24.3.18853>

Received 20 August 2017; accepted 16 November 2017

$\text{Sm}_2\text{Ti}_2\text{O}_7$  was loaded on the surface of HZSM-5 zeolite through a sol-gel route. HZSM-5 particles were coated with a thick layer of  $\text{Sm}_2\text{Ti}_2\text{O}_7$  to form the composite. It was found that crystallization of pyrochlore phase  $\text{Sm}_2\text{Ti}_2\text{O}_7$  begins at 800 °C. Continuous enlargement in  $\text{Sm}_2\text{Ti}_2\text{O}_7$  crystallite size and cell volume are accompanied with the increase of calcination temperature. The bandgap energy of the samples calcined at temperature ranging from 600 to 1000 °C was found to be around 3.4 eV. BET specific surface area and pore volume of the materials continuously decreased with rising calcination temperature. The 70 %  $\text{Sm}_2\text{Ti}_2\text{O}_7/\text{HZSM-5}$  calcined at 800 °C was found to have the greatest photocatalytic activity on RBR X-3B degradation.

**Keywords:** photocatalysis,  $\text{Sm}_2\text{Ti}_2\text{O}_7$ , calcination, sol-gel, HZSM-5.

## 1. INTRODUCTION

After nearly half a century of investigation, photocatalytic technology has become a potential advanced oxidation technique in dealing with environmental problems [1]. The focus is the synthesis of materials with strong activity on removing pollutants. The most widely studied photocatalyst is  $\text{TiO}_2$ -based material [2, 3]. Meanwhile, researchers are also interested in synthesizing titanates, e.g.  $\text{SrTiO}_3$  [4],  $\text{La}_2\text{Ti}_2\text{O}_7$  [5],  $\text{Bi}_4\text{Ti}_3\text{O}_{12}$  [6] and  $\text{CaTiO}_3$  [7].

$\text{La}_2\text{Ti}_2\text{O}_7$  was reported as a photocatalyst in environmental pollutants decomposition [8] and hydrogen evolution from water [9]. Pyrochlore structured  $\text{Sm}_2\text{Ti}_2\text{O}_7$  has also been studied for their photocatalytic activity. Masayoshi Uno reported the visible light response by  $\text{Sm}_2\text{Ti}_2\text{O}_7$  on photocatalytic generation of hydrogen [10]. Nashim prepared a composite  $\text{Sm}_2\text{Ti}_2\text{O}_7/\text{SmCrO}_3$  for photocatalytic degradation of rhodamine dyes [11]. Akio Ishikawa introduced the doping of sulfur into  $\text{Sm}_2\text{Ti}_2\text{O}_7$  to prepare  $\text{Sm}_2\text{Ti}_2\text{S}_2\text{O}_5$  for the enhanced activity on water splitting [12].

Supporting is an effective method for improving photocatalytic activity of many kinds of materials. Zeolite is a kind of material possessing porous structure and large surface area. It is utilized as adsorbent and support for many purposes. Photocatalytic activities of  $\text{TiO}_2$ ,  $\text{La}_2\text{Ti}_2\text{O}_7$  and  $\text{SrTiO}_3$  are greatly promoted after loading on HZSM-5 zeolite in our previous work [13, 14] and in the literatures [15, 16]. It is still interesting to support  $\text{Sm}_2\text{Ti}_2\text{O}_7$  on HZSM-5 zeolite. In this work,  $\text{Sm}_2\text{Ti}_2\text{O}_7$  was supported on the surface of HZSM-5 zeolite through a sol-gel route [13, 14]. The content of  $\text{Sm}_2\text{Ti}_2\text{O}_7$  in the  $\text{Sm}_2\text{Ti}_2\text{O}_7/\text{HZSM-5}$  is 70 % since it has the maximum activity. The effects of calcination temperature on the properties of the  $\text{Sm}_2\text{Ti}_2\text{O}_7/\text{HZSM-5}$  were studied. Photocatalytic oxidation

of Reactive Brilliant Red X-3B (RBR X-3B) was conducted to determine the activity of the composite.

## 2. MATERIALS AND METHODS

### 2.1. Synthesis of 70 % $\text{Sm}_2\text{Ti}_2\text{O}_7/\text{HZSM-5}$

Sol-gel method was used to synthesize samarium titanate. 1.1336 g samarium nitrate, 9 mL acetic acid and 10 mL deionized water were mixed together to form a solution. Another solution was composed of 8 mL ethanol and 0.86 mL tetrabutyl titanate. The two solutions were mixed to form a transparent precursor. The  $n(\text{Sm})/n(\text{Ti})$  molar ratio in the precursor was 1:1. HZSM-5 was added into the precursor subsequently. The mixture was stirred for about 1 h to form a sticky gel. The gel was dried at 110 °C for 15 h, and calcined for 3 h at the temperature indicated later. The obtained solid was ground and denoted as 70 %  $\text{Sm}_2\text{Ti}_2\text{O}_7/\text{HZSM-5}$ , in which the weight percentage of  $\text{Sm}_2\text{Ti}_2\text{O}_7$  was 70 %.

### 2.2. Characterization methods

X-ray diffraction patterns were recorded by a D8 Advance X-ray diffractometer. Monochromatized  $\text{Cu K}\alpha$  was chosen as the initial radiation source at  $\lambda = 1.5416\text{Å}$ . A QUANTA 250 scanning electron microscope was used to observe the surface morphology. An integrating sphere was set up on a LAMBDA 35 UV-Vis spectrometer to record UV-Vis diffuse reflectance spectra using  $\text{BaSO}_4$  as a reference. An F-sorb 3400 analyzer was used to measure specific surface area and porosity.

### 2.3. Photocatalytic degradation of RBR-X3B

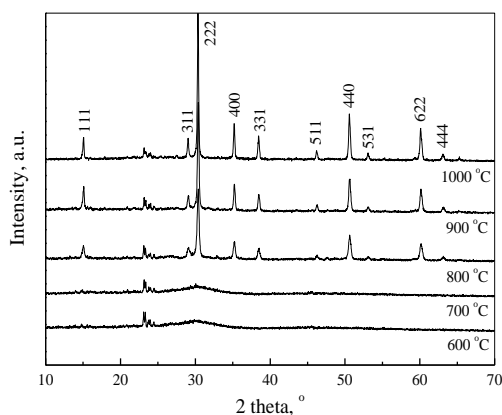
Photocatalytic activity of the 70 %  $\text{Sm}_2\text{Ti}_2\text{O}_7/\text{HZSM-5}$  composite was studied by degradation of RBR X-3B. A 100 mL quartz beaker and a 20 W UV-light lamp irradiating at  $\lambda = 253.7\text{ nm}$  were set up as the lab-scale reactor. The initial concentration of RBR X-3B aqueous solution was 30 mg/L. 20 mg 70 %  $\text{Sm}_2\text{Ti}_2\text{O}_7/\text{HZSM-5}$  and 50 mL RBR X-3B solution were stirred together for

\* Corresponding author. Tel.: +86-24-24680345.  
E-mail address: [wjzhang@aliyun.com](mailto:wjzhang@aliyun.com) (W. Zhang)

30 min in the dark to ensure adsorption-desorption equilibrium. Photocatalytic degradation of RBR X-3B started right after turning on the UV lamp. Absorbance of the RBR X-3B solution was measured at wavelength of 537.6 nm by a 721E spectrophotometer. Lambert-Beer law was used to calculate the concentration of RBR X-3B solution. UV-Vis absorption spectrum of RBR X-3B solution was recorded on a LAMBDA 35 UV-Vis spectrometer.

### 3. RESULTS AND DISCUSSION

XRD patterns of the 70 %  $\text{Sm}_2\text{Ti}_2\text{O}_7/\text{HZSM-5}$  composites are shown in Fig. 1. Calcination temperature is a key factor for  $\text{Sm}_2\text{Ti}_2\text{O}_7$  phase formation. The 70 %  $\text{Sm}_2\text{Ti}_2\text{O}_7/\text{HZSM-5}$  samples calcined below 700 °C are in amorphous state. The weak diffraction peaks between 22 – 35° are attributed to HZSM-5 zeolite. Crystallization of pyrochlore phase  $\text{Sm}_2\text{Ti}_2\text{O}_7$  begins at 800 °C. The diffraction peaks become sharper and stronger at higher calcination temperatures. The pyrochlore phase  $\text{Sm}_2\text{Ti}_2\text{O}_7$  has a Fd3m lattice in cubic crystal system. The diffraction patterns of pyrochlore phase  $\text{Sm}_2\text{Ti}_2\text{O}_7$  are in accordance to JCPDS No.73-1699. Phase transformation of  $\text{Sm}_2\text{Ti}_2\text{O}_7$  and other impurities are not observed in the figure.



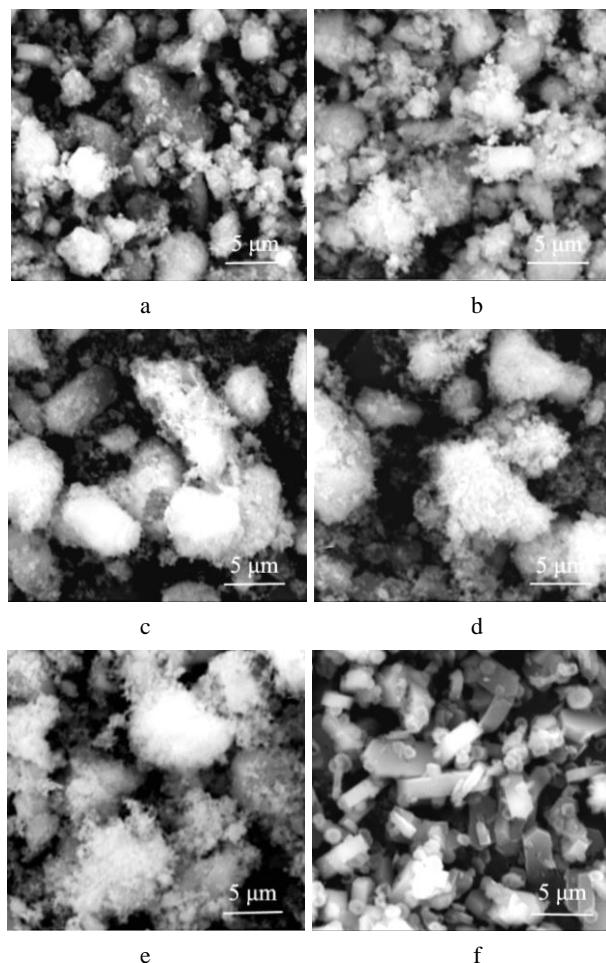
**Fig. 1.** XRD patterns of 70% $\text{Sm}_2\text{Ti}_2\text{O}_7/\text{HZSM-5}$  calcined at different temperatures

Table 1 lists lattice parameters of pyrochlore phase  $\text{Sm}_2\text{Ti}_2\text{O}_7$  in 70 %  $\text{Sm}_2\text{Ti}_2\text{O}_7/\text{HZSM-5}$  samples. A slight expansion of cell volume is accompanied with rising calcination temperature. Density of pyrochlore  $\text{Sm}_2\text{Ti}_2\text{O}_7$  slightly decreases at the same time. Scherrer formula is used to calculate crystallite size of  $\text{Sm}_2\text{Ti}_2\text{O}_7$  in the samples, based on the preferred (222) orientation [17]. The crystallite sizes are 27.6, 36.0 and 40.9 nm for the 70 %  $\text{Sm}_2\text{Ti}_2\text{O}_7/\text{HZSM-5}$  samples calcined at 800, 900 and 1000 °C. A continuous enlargement in  $\text{Sm}_2\text{Ti}_2\text{O}_7$  crystallite size is accompanied with the increase of calcination temperature.

**Table 1.** Lattice parameters of  $\text{Sm}_2\text{Ti}_2\text{O}_7$  in 70 %  $\text{Sm}_2\text{Ti}_2\text{O}_7/\text{HZSM-5}$

Temperature, °C	$a=b=c$ , $10^{-1}$ nm	$V$ , $10^{-3}$ nm <sup>3</sup>	Density, g/cm <sup>3</sup>	Crystallite size, nm
800	10.195	1059.6	6.3761	27.6
900	10.196	1059.9	6.3747	36.0
1000	10.200	1061.2	6.3667	40.9

Crystallization and crystal growing of  $\text{Sm}_2\text{Ti}_2\text{O}_7$  is favored at high temperature. SEM images of 70 %  $\text{Sm}_2\text{Ti}_2\text{O}_7/\text{HZSM-5}$  at different calcination temperatures are shown in Fig. 2. The HZSM-5 particles are in the round and regular shape.  $\text{Sm}_2\text{Ti}_2\text{O}_7$  is loaded on the surface of HZSM-5 particles in the 70 %  $\text{Sm}_2\text{Ti}_2\text{O}_7/\text{HZSM-5}$ . The shape of HZSM-5 particles is hard to be seen in the supported composites due to low HZSM-5 weight content. The weight content of  $\text{Sm}_2\text{Ti}_2\text{O}_7$  is 70% in the 70 %  $\text{Sm}_2\text{Ti}_2\text{O}_7/\text{HZSM-5}$  samples. Calcination temperature can influence the surface morphology of the composite. Crystal formation and particles aggregation during thermal treatment result in particle size growth with increasing calcination temperature.



**Fig. 2.** SEM images of 70 %  $\text{Sm}_2\text{Ti}_2\text{O}_7/\text{HZSM-5}$  at different calcination temperatures: a–600 °C; b–700 °C; c–800 °C; d–900 °C; e–1000 °C; f–HZSM-5

UV-Vis diffuse reflectance spectra of 70 %  $\text{Sm}_2\text{Ti}_2\text{O}_7/\text{HZSM-5}$  are given in Fig. 3 to show the effect of calcination temperature on bandgap energy. The bandgap energy of the sample is calculated using Kubelka-Munk theory [18] through the formula

$$(ah\nu) = A(h\nu - E_g)^n, \quad (1)$$

where  $\alpha$ ,  $h$ ,  $\nu$ ,  $A$  and  $E_g$  are the absorption coefficient, Planck constant, light frequency, proportionality constant and bandgap energy, respectively [19]. The 70 %  $\text{Sm}_2\text{Ti}_2\text{O}_7/\text{HZSM-5}$  samples have strong absorption in the UV region while the absorption edge almost does not move

when calcination temperature varies from 600 to 900 °C. The bandgap energy of the samples in this temperature range is around 3.42 eV. The bandgap energy of the samples calcined at 1000 °C slightly moves to 3.37 eV. These materials will not response to visible light irradiation. The UV lamp used in this work can irradiate at 253.7 nm. The incoming photons have enough energy to initiate the generation of electrons and holes in all the  $\text{Sm}_2\text{Ti}_2\text{O}_7$  samples.

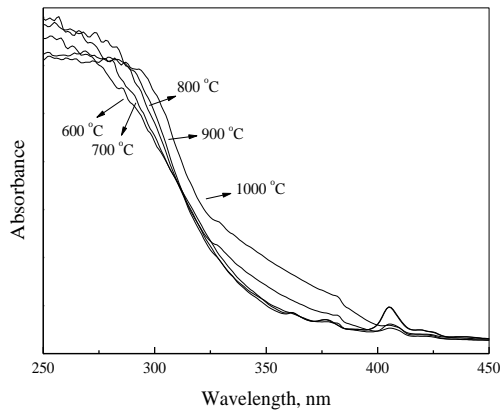


**Fig. 3.** UV-Vis diffuse reflectance spectra of 70 %  $\text{Sm}_2\text{Ti}_2\text{O}_7/\text{HZSM-5}$  samples

Fig. 4 presents  $\text{N}_2$  desorption isotherms of 70 %  $\text{Sm}_2\text{Ti}_2\text{O}_7/\text{HZSM-5}$ . The samples prepared at temperature below 800 °C contain mesopores and macropores. The isotherms of the samples are classified as IUPAC type IV for mesoporous structured material. The abrupt enlargement in adsorption capacity at  $\text{N}_2$  relative pressure over 0.9 is due to the interparticle macropores. The  $\text{N}_2$  adsorption amount on these samples are much larger than the samples calcined at 900 °C and 1000 °C. Adsorption of  $\text{N}_2$  molecules on the two latter materials is very weak in the whole  $\text{N}_2$  relative pressure range.

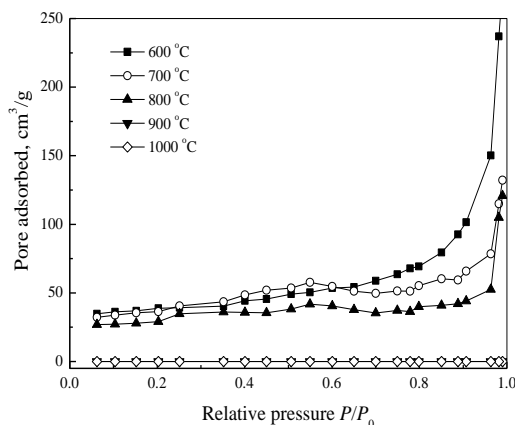


**Fig. 4.**  $\text{N}_2$  desorption isotherms of 70%  $\text{Sm}_2\text{Ti}_2\text{O}_7/\text{HZSM-5}$  calcined at different temperatures

Specific surface area and porous properties of 70 %  $\text{Sm}_2\text{Ti}_2\text{O}_7/\text{HZSM-5}$  are given in Table 2. BET specific surface area of the materials continuously decreases with rising calcination temperature. Crystalline growth and particles aggregation during high temperature thermal treatment are the main reasons. The sample at 600 °C has the maximum specific surface area of 173  $\text{m}^2/\text{g}$  and the

largest pore volume of 0.413  $\text{cm}^3/\text{g}$ . Organic substances in the gel were burnt out during calcination, leaving porous structure in the material.

The 70 %  $\text{Sm}_2\text{Ti}_2\text{O}_7/\text{HZSM-5}$  is composed of 70 %  $\text{Sm}_2\text{Ti}_2\text{O}_7$  and 30 % HZSM-5. The specific surface of HZSM-5 is 223.8  $\text{m}^2/\text{g}$ . The average pore size and total pore volume in HZSM-5 zeolite powder are 1.91 nm and 0.1068  $\text{cm}^3/\text{g}$ , respectively. The HZSM-5 is quite thermal-stable that the above-mentioned data are almost unchanged after thermal treating. As a result, the variations in surface area and porous properties of 70 %  $\text{Sm}_2\text{Ti}_2\text{O}_7/\text{HZSM-5}$  are mainly attributed to the supported  $\text{Sm}_2\text{Ti}_2\text{O}_7$ , but not the HZSM-5 zeolite. On the other hand, since the HZSM-5 particles are coated with a thick layer of  $\text{Sm}_2\text{Ti}_2\text{O}_7$ , the micropores in the zeolite can also be blocked by  $\text{Sm}_2\text{Ti}_2\text{O}_7$ .

**Table 2.** Specific surface area and porous properties of 70 %  $\text{Sm}_2\text{Ti}_2\text{O}_7/\text{HZSM-5}$

Temperature, °C	BET surface area, $\text{m}^2/\text{g}$	Average pore size, nm	Pore volume, $\text{cm}^3/\text{g}$
600	173	13.1	0.413
700	145	4.8	0.208
800	132	5.4	0.179
900	93	6.2	0.167
1000	80	6.0	0.120

The effects of calcination temperature on adsorption and photocatalytic degradation of RBR X-3B on 70 %  $\text{Sm}_2\text{Ti}_2\text{O}_7/\text{HZSM-5}$  are shown in Fig. 5. More than half of the dye can be removed after adsorption-desorption equilibrium on the samples prepared at temperature below 700 °C. This is due to the large specific surface area and pore volume in these samples. The adsorption capacity of the materials declines drastically with increasing calcination temperature as the result of shrinking surface area and porosity.

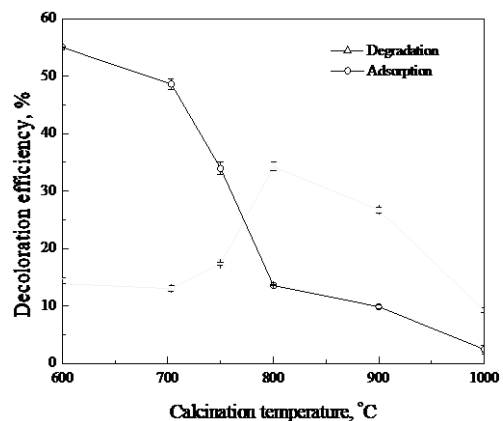


**Fig. 5.** Effects of calcination temperature on adsorption and photocatalytic degradation of RBR X-3B on 70 %  $\text{Sm}_2\text{Ti}_2\text{O}_7/\text{HZSM-5}$ . The irradiation time was 30 min

On the contrast, the samples calcined below 700 °C have poor activity on photocatalytic degradation of RBR X-3B. The active crystallite  $\text{Sm}_2\text{Ti}_2\text{O}_7$  does not form at low temperature. The 70 %  $\text{Sm}_2\text{Ti}_2\text{O}_7/\text{HZSM-5}$  sample calcined at 800 °C has the maximum photocatalytic activity, while further increase of calcination temperature leads to a continuous declining of the activity. Crystallization and surface character are the two major

factors influencing the adsorption capacity and photocatalytic activity of the composite materials.

Fig. 6 gives the UV-Vis absorption spectra of RBR X-3B solution with extending illumination. The 70 %  $\text{Sm}_2\text{Ti}_2\text{O}_7/\text{HZSM-5}$  sample calcined at 800 °C was used as the photocatalyst. RBR X-3B solution has absorptions in both visible and UV regions. The red color of the solution comes from the conjugated chromophore in RBR X-3B molecule. The chromophore group has the maximum absorption intensity at 537.6 nm in the visible region. The removal of the dye from solution is recorded by measuring the absorption intensity at this wavelength.

RBR X-3B solution also has strong absorptions in the UV region centering at 230, 280 and 315 nm, corresponding to triazine ring, naphthalene ring and benzene ring. Intensities of all the absorption peaks constantly decline with prolonged illumination time. The broad peak between 450 and 570 nm almost disappears after 120 min of irradiation, indicating the degradation of the dye. The first order kinetic reaction constant is  $0.01723 \text{ min}^{-1}$  on the 70 %  $\text{Sm}_2\text{Ti}_2\text{O}_7/\text{HZSM-5}$  sample calcined at 800 °C. At the same time, there are still apparent absorptions in the UV region. The triazine ring and naphthalene ring are hard to be decomposed.

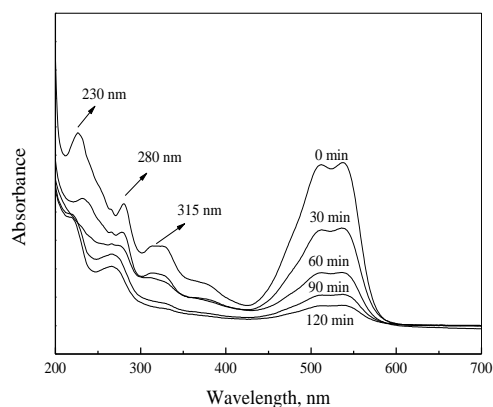


**Fig. 6.** UV-Vis absorption spectra of RBR X-3B solution during irradiation in presence of 70 %  $\text{Sm}_2\text{Ti}_2\text{O}_7/\text{HZSM-5}$  calcined at 800 °C

#### 4. CONCLUSIONS

The effects of calcination on the properties of the supported 70 %  $\text{Sm}_2\text{Ti}_2\text{O}_7/\text{HZSM-5}$  were studied. Pyrochlore phase  $\text{Sm}_2\text{Ti}_2\text{O}_7$  begins to form over 800 °C. The cell volume slightly expands with rising calcination temperature. The 70 %  $\text{Sm}_2\text{Ti}_2\text{O}_7/\text{HZSM-5}$  samples have strong absorption in the UV region with bandgap energy around 3.4 eV. The surface area and pore volume of 70 %  $\text{Sm}_2\text{Ti}_2\text{O}_7/\text{HZSM-5}$  drop off with increasing calcination temperature. The adsorption capacity of the materials drastically declines at high calcination temperature. The 70 %  $\text{Sm}_2\text{Ti}_2\text{O}_7/\text{HZSM-5}$  sample calcined at 800 °C has the maximum photocatalytic activity.

#### REFERENCES

1. Zhang, W.J., Ma, Z., Li, K.X., Yang, L.L., Li, H., He, H.B. Sol-gel Synthesis of Nano-sized  $\text{TiO}_2$  Supported on HZSM-5 *Current Nanoscience* 12 2016: pp. 514–519.

<https://doi.org/10.2174/1573413712666151223201637>

2. Pang, D., Qiu, L., Wang, Y., Zhu, R., Ouyang, F. Photocatalytic Decomposition of Acrylonitrile with N-F Codoped  $\text{TiO}_2/\text{SiO}_2$  under Simulant Solar Light Irradiation *Journal of Environmental Science* 33 2015: pp. 169–178. <https://doi.org/10.1016/j.jes.2015.01.017>
3. Zhang, W.J., Li, C.G., Ma, Z., Yang, L.L., He, H.B. Effects of Calcination Temperature on Properties of 0.5 % Al-3 % In- $\text{TiO}_2$  Photocatalyst Prepared using Sol-Gel Method *Journal of Advanced Oxidation Technology* 19 2016: pp. 119–124. <https://doi.org/10.1515/jaots-2016-0116>
4. Li, F., Yu, K., Lou, L., Su, Z., Liu, S. Theoretical and Experimental Study of La/Ni Co-doped  $\text{SrTiO}_3$  Photocatalyst *Materials Science and Engineering: B* 172 2010: pp. 136–141. <https://doi.org/10.1016/j.mseb.2010.04.036>
5. Chen, J., Liu, S., Zhang, L., Chen, N. New  $\text{SnS}_2/\text{La}_2\text{Ti}_2\text{O}_7$  Heterojunction Photocatalyst with Enhanced Visible-Light Activity *Materials Letters* 150 2015: pp. 44–47. <https://doi.org/10.1016/j.matlet.2015.02.134>
6. Chen, Z., Jiang, H., Jin, W., Shi, C. Enhanced Photocatalytic Performance over  $\text{Bi}_4\text{Ti}_3\text{O}_{12}$  Nanosheets with Controllable Size and Exposed  $\{0\ 0\ 1\}$  Facets for Rhodamine B degradation *Applied Catalysis B* 180 2016: pp. 698–706. <https://doi.org/10.1016/j.apcatb.2015.07.022>
7. Lozano-Sánchez, L.M., Obregón, S., Díaz-Torres, L.A., Lee, S., Rodríguez-González, V. Visible and Near-Infrared Light-Driven Photocatalytic Activity of Erbium-Doped  $\text{CaTiO}_3$  System *Journal of Molecular Catalysis A* 410 2015: pp. 19–25. <https://doi.org/10.1016/j.molcata.2015.09.005>
8. Li, Y., Chen, G., Zhang, H., Li, Z., Sun, J. Electronic Structure and Photocatalytic Properties of  $\text{ABi}_2\text{Ta}_2\text{O}_9$  (A=Ca, Sr, Ba) *Journal of Solid State Chemistry* 181 2008: pp. 2653–2659. <https://doi.org/10.1016/j.jssc.2008.05.020>
9. Hwang, D., Kim, H., Lee, J., Kim, J., Li, W., Oh, S. Photocatalytic Hydrogen Production from Water over M-Doped  $\text{La}_2\text{Ti}_2\text{O}_7$  (M=Cr, Fe) under Visible Light Irradiation ( $\lambda > 420 \text{ nm}$ ) *Journal of Physical Chemistry B* 109 2005: pp. 2093–2102. <https://doi.org/10.1021/jp0493226>
10. Uno, M., Kosuga, A., Okui, M., Horisaka, K., Yamanaka, S. Photoelectrochemical Study of Lanthanide Titanium Oxides,  $\text{Ln}_2\text{Ti}_2\text{O}_7$  (Ln = La, Sm, and Gd) *Journal of Alloys and Compounds* 400 2005: pp. 270–275. <https://doi.org/10.1016/j.jallcom.2005.04.004>
11. Nashim, A., Parida, K.M. Novel  $\text{Sm}_2\text{Ti}_2\text{O}_7/\text{SmCrO}_3$  Heterojunction Based Composite Photocatalyst for Degradation of Rhodamine 6G Dye *Chemical Engineering Journal* 215–216 2013: pp. 608–615. <https://doi.org/10.1016/j.cej.2012.11.025>
12. Ishikawa, A., Takata, T., Matsumura, T., Kondo, J.N., Hara, M., Kobayashi, H., Domen, K. Oxysulfides  $\text{Ln}_2\text{Ti}_2\text{S}_2\text{O}_5$  as Stable Photocatalysts for Water Oxidation and Reduction under Visible-Light Irradiation *Journal of Physical Chemistry B* 108 2004: pp. 2637–2642. <https://doi.org/10.1021/jp036890x>
13. Zhang, W.J., Bi, F.F., Yu, Y., He, H.B. Phosphoric Acid Treating of ZSM-5 Zeolite for the Enhanced Photocatalytic Activity of  $\text{TiO}_2/\text{HZSM-5}$  *Journal of Molecular Catalysis A* 372 2013: pp. 6–12.

- <https://doi.org/10.1016/j.molcata.2013.02.002>
14. **Zhang, W., Du, L., Bi, F., He, H.** A Novel SrTiO<sub>3</sub>/HZSM-5 Photocatalyst Prepared by Sol-Gel Method *Materials Letters* 157 2015: pp. 103–105.  
<https://doi.org/10.1016/j.matlet.2015.05.056>
  15. **Guo, P., Wang, X.S., Guo, H.C.** TiO<sub>2</sub>/Na-HZSM-5 Nano-Composite Photocatalyst: Reversible Adsorption by Acid Sites Promotes Photocatalytic Decomposition of Methyl Orange *Applied Catalysis B* 90 2009: pp. 677–687.  
<https://doi.org/10.1016/j.apcatb.2009.04.028>
  16. **Kumari, V., Subrahmanyam, M., Subba, K., Ratnamala, A., Noorjahan, M., Tanaka, K.** An Easy and Efficient Use of TiO<sub>2</sub> Supported HZSM-5 and TiO<sub>2</sub>+HZSM-5 Zeolite Combine in the Photodegradation of Aqueous Phenol and P-chlorophenol *Applied Catalysis A* 234 2002: pp. 155–165.  
[https://doi.org/10.1016/S0926-860X\(02\)00224-7](https://doi.org/10.1016/S0926-860X(02)00224-7)
  17. **Li, L., Ma, Z., Bi, F., Li, H., Zhang, W., He, H.** Sol-gel Preparation and Properties of Bi<sub>4</sub>Ti<sub>3</sub>O<sub>12</sub> Photocatalyst Supported on Micrometer-Sized Quartz Spheres *Journal of Advanced Oxidation Technology* 19 2016: pp. 310–316.  
<https://doi.org/10.1515/jaots-2016-0215>
  18. **Kubelka, P., Munk, F.Z.** Ein Beitrag zur Optik der Farbanstriche *Technical Physics* 12 1931: pp. 593–601.
  19. **Butler M.A.** Photoelectrolysis and Physical Properties of the Semiconducting Electrode WO<sub>2</sub> *Journal of Applied Physics* 48 1977: pp. 1914–1919.  
<https://doi.org/10.1063/1.323948>